© 2017. Published by The Company of Biologists Ltd | Journal of Experimental Biology (2017) 220, 1882-1893 doi:10.1242/jeb.155416

RESEARCH ARTICLE

Inverse dynamic modelling of jumping in the red-legged running frog, *Kassina maculata*

Laura B. Porro[1,*], Amber J. Collings[1], Enrico A. Eberhard[1], Kyle P. Chadwick[2] and Christopher T. Richards[1]

ABSTRACT

Although the red-legged running frog, *Kassina maculata*, is secondarily a walker/runner, it retains the capacity for multiple locomotor modes, including jumping at a wide range of angles (nearly 70 deg). Using simultaneous hind limb kinematics and single-foot ground reaction forces, we performed inverse dynamics analyses to calculate moment arms and torques about the hind limb joints during jumping at different angles in *K. maculata.* We show that forward thrust is generated primarily at the hip and ankle, while body elevation is primarily driven by the ankle. Steeper jumps are achieved by increased thrust at the hip and ankle and greater downward rotation of the distal limb segments. Because of its proximity to the GRF vector, knee posture appears to be important in controlling torque directions about this joint and, potentially, torque magnitudes at more distal joints. Other factors correlated with higher jump angles include increased body angle in the preparatory phase, faster joint openings and increased joint excursion, higher ventrally directed force, and greater acceleration and velocity. Finally, we demonstrate that jumping performance in *K. maculata* does not appear to be compromised by presumed adaptation to walking/running. Our results provide new insights into how frogs engage in a wide range of locomotor behaviours and the multi-functionality of anuran limbs.

KEY WORDS: Locomotion, Biomechanics, Joint angles, Force plate, Inverse dynamic analysis

INTRODUCTION

Animals jump to move through their environment, escape predators and capture prey (Alexander, 1995; Biewener, 2003). Jumping is the dominant mode of terrestrial locomotion in anurans (Emerson, 1978), involving explosive movement from a stationary, crouched posture and potentially utilizing elastic pre-loading of tendons (Peplowski and Marsh, 1997; Roberts and Marsh, 2003; Astley and Roberts, 2014). Anuran jumping has been studied using a variety of techniques, nearly all of which have focused on taxa thought to be specialized hoppers and jumpers (Calow and Alexander, 1973; Kamel et al., 1996; Lutz and Rome, 1996b; Gillis and Biewener, 2000; Wilson et al., 2000; Kargo et al., 2002; Azizi and Roberts, 2010; Astley and Roberts, 2011). Adaptation for jumping is thought to be reflected in anuran skeletal morphology. Compared with salamanders, anurans feature elongated hind limbs, tibiofibular fusion, elongated ilia, fusion of the caudal vertebrae into a urostyle, reduction in the number of presacral vertebrae and mobility at the sacroiliac and sacro-urostylic joints (Alexander, 1995; Jenkins and Shubin, 1998; Reilly and Jorgensen, 2011). However, anurans engage in locomotor behaviours other than jumping, and skeletal morphology in some groups may be adapted for these modes (Emerson, 1979, 1982; Reilly and Jorgensen, 2011). For example, variations in relative limb lengths have been associated with differential jumping ability (Zug, 1972), and both Emerson (1979, 1982) and Reilly and Jorgensen (2011) associated variations in pelvic musculoskeletal morphology with diverse locomotor behaviours. Reilly and Jorgensen (2011) even suggested walking – not jumping – as the basal anuran locomotor mode.

Kassina maculata (Duméril 1853) (red-legged running frog) is a secondary walker – despite belonging to the arboreal Hyperoliidae, *K. maculata* uses a walking/running gait as its primary locomotor mode (Ahn et al., 2004; Danos and Azizi, 2015). However, *K. maculata* also climbs, burrows, swims and jumps (Loveridge, 1976; McAllister and Channing, 1983). We recorded 3D limb and body kinematics in *K. maculata* while simultaneously collecting single-foot forces exerted during jumping at a wide range of angles. These data were used to carry out inverse dynamics analysis and calculate the external moments acting about the hind limb joints during jumping in a walking (as opposed to jumping) frog taxon for the first time. We hypothesize that, based on kinematics analysis (Richards et al., 2017), forward thrust is produced by hip, knee and ankle extension whereas elevation is produced at the ankle and knee; it is at these joints that we expect fine-tuning of jump angle to be achieved. Specifically, steeper jump angles require higher ankle and knee torques to drive downward rotation of the distal limb elements to elevate the body.

MATERIALS AND METHODS

Animal husbandry

Data were collected from four adult *K. maculata* with mean (±s.d.) body mass of 28.4±3.7 g and a mean snout–vent length (SVL) of 60.0±1.2 mm (see Table S1 for full information) obtained from commercial suppliers (AmeyZoo, Bovingdon, UK) and housed in the Biological Services Unit at the Royal Veterinary College, Hatfield, UK. Animals were housed in 45×45×45 cm terrariums (Exo Terra, Montreal, Canada) in a temperature-controlled room set at 19–26°C and 25–60% relative humidity on a 12 h:12 h reversed light:dark cycle. Terrariums contained vegetation, hiding places, a small pool and a substrate of coco fibre, and were misted twice daily. Frogs were fed crickets, waxworms and bloodworms three times per week; once a week, crickets were dusted with mineral powder. All husbandry and experimental procedures were in accordance with UK Home Office regulations (Licence 70/8242) and Royal Veterinary College Ethics and Welfare Committee.

[1]Structure and Motion Laboratory, Department of Comparative Biomedical Sciences, Royal Veterinary College, Hawkshead Lane, Hatfield AL9 7TA, UK. [2]Children's Hospital Los Angeles, University of Southern California, 4650 Sunset Boulevard, Los Angeles, CA 90027, USA.

*Author for correspondence (lporro@rvc.ac.uk)

L.B.P., 0000-0002-0546-2381

Received 22 December 2016; Accepted 2 March 2017

Journal of Experimental Biology

Journal of Experimental Biology (2017) 220, 1882-1893 doi:10.1242/jeb.155416

Data collection

External skin markers were made by cutting white plastic circles using a screw punch (Nonaka Mfg. Co. Ltd., Japan) with a 5 mm hollow point drill bit; these circles were painted on one side with a black marker. Seven markers were applied to anatomical landmarks on the body and the left hind limb using cyanoacrylate adhesive (Fig. 1A). Forces exerted during jumping were recorded using a Nano17 force/torque transducer (ATI Industrial Automation, Apex, NC, USA) mounted in a purpose-built trackway. To record single-foot forces, a small stiff aluminium plate (flush with the trackway surface) was rigidly fixed to the load cell, providing sufficient area for foot contact. Force data during jumping were acquired at 2000 Hz with acquisition to a PC (NI-6289) controlled by a custom-written LabVIEW (National Instruments, Austin, TX, USA) script. Frogs were simultaneously filmed at 250 frames s^{-1} at a 1/1500 s shutter speed using two high-speed Photron FASTCAM cameras (Photron Ltd, San Diego, CA, USA) positioned dorsal and lateral to the force plate; an angled mirror placed opposite the lateral camera at 60 deg from the horizontal was used to obtain a third view. A custom-built 49-point calibration object was used to calibrate the three views. Video data were acquired using the Photron FASTCAM Viewer and synchronized with force data using a post-trigger. Both the cameras and force transducer used a right-handed global reference frame in which the *X*-axis (mediolateral) pointed right, the *Y*-axis (fore–aft) pointed forward and the *Z*-axis (dorsoventral) pointed up (Fig. 1A). Frogs were positioned with the marked left hind leg resting on the force plate (to obtain single-foot forces) and facing the lateral camera, and were encouraged to jump forwards (positive *Y*) to a dark box by sudden movements or gentle tapping of the unmarked hind foot. A range of jump angles were elicited by varying the height of the box. Trials were conducted at 22.5°C. After experiments, animals were weighed and measured, and markers were gently removed.

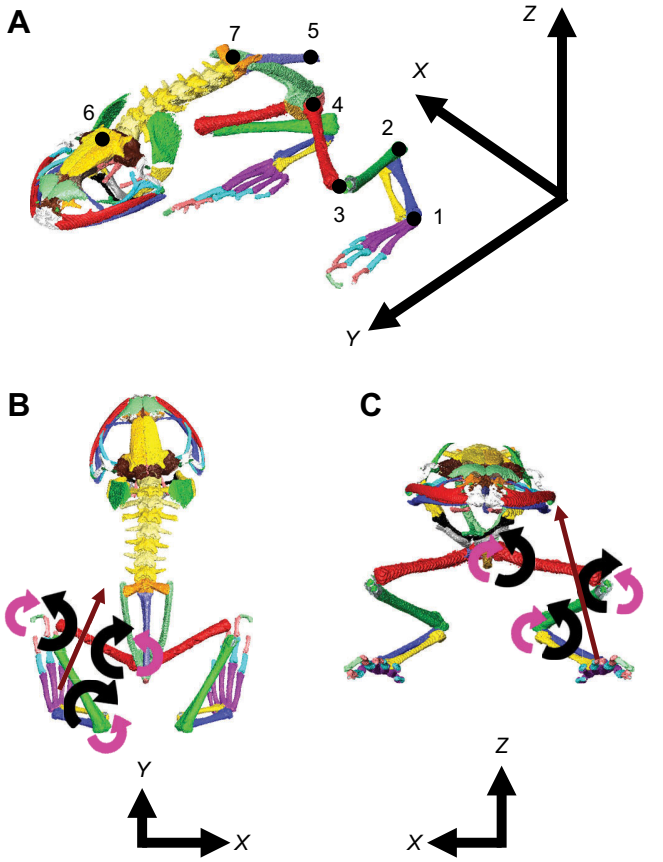

Fig. 1. Marker position, global coordinate system and torque directions. Three-dimensional skeletal model of *Kassina maculata* (from CT scans) in oblique (A), dorsal (B) and anterior (C) views. Global coordinate systems shown; in B and C, the *Z*- and *Y*-axes (respectively) are coming out of the page. Black dots mark the positions of the tarsometatarsal (TMT) (1), ankle (2), knee (3), hip (4), vent (5), head (6) and sacral (7) kinematic markers in A. In B and C, dark red arrows show the approximate orientation of the ground reaction force midway through a jump; curved black arrows show the directions of the external torques (generated by ground reaction force) on the ankle, knee and hip joints; curved pink arrows show the directions of the opposing muscle torques required to balance external torques.

Data extraction and processing

Kinematic data from the three views were calibrated and markers were digitized to *XYZ* coordinates using open source script (Hedrick, 2008) in MATLAB (MathWorks, Natick, MA, USA). An eighth point representing the estimated centre of pressure (COP) of the marked foot was digitized. It was assumed that the *Y* (fore–aft) position of the COP was the most posterior point of the foot contacting the substrate in each frame and its *X* (mediolateral) location was along the foot midline.

Force and kinematic data were processed and analyzed using custom-written scripts in Mathematica 10.0 (Wolfram Research, Champaign, IL, USA). Strain output from the transducer was converted to *XYZ* components of the force exerted by the frog using a factory-supplied calibration and zeroed at take-off. Both *XYZ* coordinate and force data were smoothed by a second-order reverse Butterworth low-pass filter using a cut-off frequency of 25 Hz; data were not filtered further. Although only non-turning jumps were included in our analyses (see below), frogs rarely jumped exactly parallel to the *Y*-axis. An axis defined by the cranial and vent markers (**B**) was used to calculate yaw angle (α) of the frog relative to the *Y*-axis (**Y**), defined as [0,1,0]:

$$\alpha = \cos^{-1}\frac{\mathbf{B}\cdot\mathbf{Y}}{\|\mathbf{B}\|\cdot\|\mathbf{Y}\|}, \quad (1)$$

in which $\cdot$ denotes the dot product. The calculated yaw angles were cancelled via a rotation matrix (**R**) about the *Z*-axis:

$$\mathbf{R} = \begin{bmatrix} \cos(\alpha) & -\sin(\alpha) & 0 \\ \sin(\alpha) & \cos(\alpha) & 0 \\ 0 & 0 & 1 \end{bmatrix}. \quad (2)$$

Thus, for each frame, the 8 (markers)×3 (*XYZ* coordinates) kinematic data matrix (**M**) was rotated about the *Z*-axis so that the body axis of the frog was aligned with the *Y*-axis throughout the jump (**M′**):

$$\mathbf{M}' = (\mathbf{R}^{\mathbf{T}}\cdot\mathbf{M}^{\mathbf{T}})^{\mathbf{T}}, \quad (3)$$

in which **T** is the matrix transpose. This rotation matrix was also applied to the *XYZ* force components. Lastly, force data were down-sampled to synchronize with the kinematic data.

Force plate measurements were used to quantify maximum vertical, fore–aft and mediolateral forces, as well as maximum resultant force (both absolute and relative to body mass) and the times at which they occurred, which are presented in Table 1, Table S2 and Fig. 2. Kinematic data were used to quantify the magnitude and timing of maximum velocity – absolute and relative to SVL – and maximum acceleration measured at the hip marker, which is closest to the frog's centre of mass (COM). Take-off angle was defined as the *YZ* angle of the velocity vector (of the hip marker) relative to the *Y*-axis. Our video setup did not capture the animals

Journal of Experimental Biology (2017) 220, 1882-1893 doi:10.1242/jeb.155416

Table 1. Mean peak force magnitudes, ratios and timings (data from a single foot unless indicated); average peak velocity and acceleration, and timings; mean jump angles and distance

Subject	Mean peak DV force (N)	Mean peak AP force (N)	Mean peak total force (N)	Total force/body weight	DV/AP force magnitude	DV/AP force time (ratio)	Peak force time (s)
KM03	−0.25±0.08	−0.13±0.02	0.38±0.11	3.04±0.791	1.94±0.66	0.98	−0.06
KM04	−0.24±0.09	−0.16±0.04	0.36±0.12	2.92±0.99	1.58±0.55	0.93	−0.06
KM05	−0.30±0.08	−0.21±0. 04	0.48±0.12	2.80±0.73	1.47±0.49	0.99	−0.05
KM06	−0.28±0.07	−0.20±0.03	0.45±0.10	3.24±0.72	1.47±0.52	0.96	−0.04
All trials	−0.27±0.09	−0.17±0.04	0.41±0.12	3.03±0.87	1.62±0.59	0.96	−0.06

Subject	Mean peak velocity (m s^{-1})	Mean peak SVL s^{-1}	Mean peak acceleration (m s^{-2})	Peak velocity time (s)	Peak acceleration time (s)	Jump angle (deg)	Jump distance (m)
KM03	1.20±0.30	20.7±5.2	32.6±8.1	−0.02	−0.06	34±24	0.14±0.07
KM04	1.32±0.34	21.9±5.7	31.3±11.1	−0.02	−0.06	30±21	0.18±0.09
KM05	1.47±0.20	24.1±3.3	38.3±17.1	−0.01	−0.06	36±15	0.24±0.07
KM06	1.46±0.12	24.0±2.0	40.7±9.9	−0.01	−0.07	36±11	0.23±0.06
All trials	1.36±0.28	22.6±4.6	35.6±12.1	−0.01	−0.06	34±19	0.19±0.09
Max.	2.02	33.1	79.5			69	0.34
Min.	0.67	11.0	15.7			0.3	0.03

DV, dorsoventral; AP, anteroposterior. Total force scaled to body weight accounts for forces from both hind limbs. Peak timings assume take-off occurs at time=0.

landing; thus, jump distance (**D**) was modelled using the following ballistic equations (Eqns 4 and 5). Horizontal and vertical distance travelled through time were calculated as:

$$\mathbf{D}_{\mathrm{Y}} = \mathbf{V}_{\mathrm{Y}} \times t, \quad (4)$$

$$\mathbf{D}_{\mathrm{Z}} = \mathbf{V}_{\mathrm{Z}} \times t - 0.5 \times \boldsymbol{g} \times t^2 + \mathbf{H}_{\mathrm{COM}}, \quad (5)$$

in which t is time after take-off, $\mathbf{D}_{\mathrm{Y}}$ is horizontal displacement, $\mathbf{D}_{\mathrm{Z}}$ is vertical displacement, $\mathbf{V}_{\mathrm{Y}}$ is the forward (Y) velocity at take-off, $\mathbf{V}_{\mathrm{Z}}$ is the vertical (Z) velocity at take-off, $\boldsymbol{g}$ is acceleration due to gravity (9.8 m s^{-2}) and $\mathbf{H}_{\mathrm{COM}}$ is the height of the COM at take-off. We calculated total flight time by solving for $\mathbf{D}_{\mathrm{Z}}$ crossing zero – representing impact – and used this to solve for horizontal distance travelled. Kinematic performance metrics are presented in Table 1 and Table S2.

Kinematic markers were used as a proxies for joint centres of rotation and endpoints of limb segments. Instantaneous 3D axes of rotation ($\mathbf{J}_{\mathrm{Axis}}$) were determined for the ankle, knee, hip and sacroiliac joints using the vectors defined by the joint marker and endpoint of the proximal segment ($\mathbf{V}_{\mathrm{Prox}}$), and by the joint marker and endpoint of the distal segment ($\mathbf{V}_{\mathrm{Dist}}$) in Eqn 6:

$$\mathbf{J}_{\mathrm{Axis}} = \left(\cos^{-1}\frac{\mathbf{V}_{\mathrm{Prox}} \cdot \mathbf{V}_{\mathrm{Dist}}}{\| \mathbf{V}_{\mathrm{Prox}} \cdot \mathbf{V}_{\mathrm{Dist}} \|}\right) \times \mathrm{Norm}\ (\mathbf{V}_{\mathrm{Prox}} \times \mathbf{V}_{\mathrm{Dist}}) \times -1, \quad (6)$$

in which × denotes the cross-product. The norm of this 3D axis vector gives the 3D joint angles. Body angle was defined as the YZ angle formed between the head and vent markers, and the Y-axis. Maximum, minimum and range of joint angles and peak joint angular velocities are presented in Table 2, Fig. 3 and Table S2.

Force and kinematic data were used in inverse dynamics analyses to estimate external moment arms and torques acting at the hip, knee, ankle and tarsometatarsal (TMT) joints during jumping (Table 3, Figs 4, 5, Table S2). Three-dimensional external moment arm vectors ($\mathbf{V}_{\mathrm{MA}}$) were calculated using vectors defined by the COP and GRF ($\mathbf{V}_{\mathrm{GRF}}$) and by the COP and joint ($\mathbf{V}_{\mathrm{Joint}}$) (Weisstein, 2009):

$$\mathbf{V}_{\mathrm{MA}} = \| \mathbf{V}_{\mathrm{GRF}} \times \mathbf{V}_{\mathrm{Joint}} \| / \| \mathbf{V}_{\mathrm{GRF}} \|. \quad (7)$$

The norm of $\mathbf{V}_{\mathrm{MA}}$ gives the magnitude of the external moment arm. The XYZ components of the external torques ($\mathbf{V}_{\mathrm{Torque}}$) at each joint in world space were calculated by:

$$\mathbf{V}_{\mathrm{Torque}} = \mathbf{V}_{\mathrm{MA}} \times \mathbf{GRF}, \quad (8)$$

in which **GRF** is the GRF vector. The norm of $\mathbf{V}_{\mathrm{Torque}}$ is the magnitude of the 3D external torque. The norms of the XY and XZ components give torque magnitudes about the Z- and Y-axes, respectively, permitting us to evaluate contributions to limb protraction/retraction (i.e. anterior/posterior rotation) versus abduction/adduction (i.e. dorsal/ventral rotation) (Fig. 5, Table 3, Table S2). Positive (counterclockwise) XY torques indicate that the GRF acts to retract the limb segment; positive XZ torques indicate the GRF acts to abduct the limb segment (Fig. 1B,C). Internal torques generated by the frog's muscles in either plane must counteract external torques. Therefore, to facilitate further discussion, we will refer to joint torques from the muscles' point of view: negative XY torques retract limb segments whereas positive XZ torques adduct segments (Fig. 1B,C).

In addition to being analyzed in absolute time, data were normalized by percent of jump contact time for comparison and statistical analyses (Figs 2–5, Figs S1, S2). The end of each jump (in which the last toe left ground) was defined as take-off. Jump start was defined as the onset of velocity at the hip marker (closest to the COM; see Richards et al., 2017). Within this interval (i.e. jump start to take-off), data were resampled to 100 points using interpolation. Performance metrics were also plotted relative to take-off angle (Fig. 3), with trials classified as low, intermediate and high jumps by separating take-off angles into quantiles: low jumps include take-off angles below the first quantile (n=13, ranging from 0 to 20 deg); intermediate jumps include take-off angles between the first and third quantiles (n=24, from 21 to 49 deg); and high jumps include take-off angles above the third quantile (n=13, from 50 to 70 deg).

Statistical tests

Statistical tests were performed in Mathematica. General linear models (specifically, ANCOVAs) were used to investigate the relationship between jump angle (the dependent, continuous variable), individual frog (a categorical covariate) and the following separate continuous covariate performance metrics: maximum vertical, anteroposterior and total (scaled to body weight) exerted forces; maximum velocity and acceleration; 3D joint and body angles (range and maximum); maximum 3D external

Journal of Experimental Biology (2017) 220, 1882-1893 doi:10.1242/jeb.155416

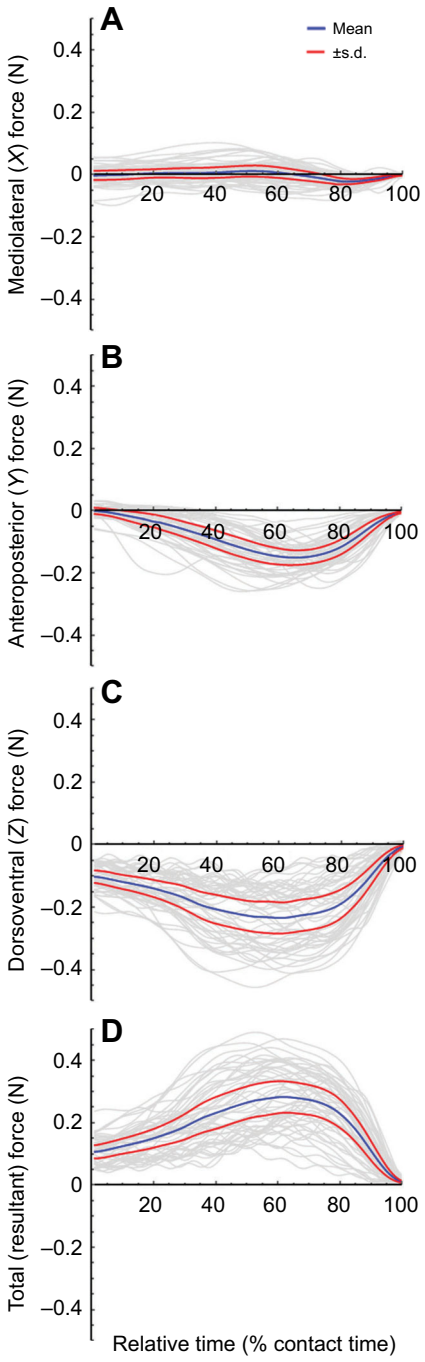

Fig. 2. Single-foot forces exerted during jumping in *Kassina maculata*. Data from 50 trials and four individuals are normalized and resampled to 100 time points using methods described in the text and shown to the same scale for all trials (A–D), including mediolateral (A), anteroposterior (B), dorsoventral (C) and total resultant (D) forces. Blue traces indicate mean force values; red traces indicate standard deviation; traces for individual trials are shown in grey.

moment arms; and maximum 3D, *XY* and *XZ* moments (Table S3). We also tested for interaction effects between individuals and the covariate performance variables, and used a significance threshold of P=0.05 for the regression component.

CT scanning

One individual was scanned using micro-computed tomography (μCT) at the Cambridge Biotomography Centre (University of Cambridge, UK) on an X-Tek H 225 μCT scanner (Nikon Metrology, Tring, UK) at 65 kV and 340 μA producing 1158 TIFF images with a resolution of 0.0493 mm voxel^{-1}. Scans were processed in Avizo 8.0 (FEI, Hillsboro, OR, USA) producing 3D models of the bones and soft tissues of the left foot, tarsus, shank, thigh, and body (pelvis–abdominal–thoracic segment, head and fore limbs). The long-axis of each segment was aligned with the global *Y*-axis and the proximal joint of each segment (vent of the body segment) directed towards the origin; the dorsal aspect of each segment was directed towards positive *Z*. A custom-written MATLAB script (Allen et al., 2013) was used to calculate mass, COM location and moments of inertia about all axes for each segment (the latter two measured from the proximal joint), assuming a density of 1.93 g cm^{-3} for bone and 1.056 g cm^{-3} for soft tissue (Biltz and Pellegrino, 1969) (Table S1). Three-dimensional surfaces were used to create figures and a 3D model (Fig. S3) using Tetra4D Reviewer (Tech Soft 3D, Bend, OR, USA) and Adobe Acrobat Pro X (Adobe Systems Inc., San Jose, CA, USA).

Sensitivity analyses

The position of the COP was estimated to account for its movement as the foot peels off the ground during take-off. We tested the sensitivity of our results to alternate COP locations for three trials: KM04 HOP 12, KM04 HOP 09 and KM04 HOP 14 (low, intermediate and high-angle jumps, respectively). A random point between the estimated COP (most posterior point of the left foot contacting the ground) and the distal tip of the fourth toe (the last to leave the ground) was selected for each time frame; this was repeated 100 times for each trial, and torques about joints were calculated and compared with those produced using our estimated COP (Fig. S1).

To understand the impact of limb inertial properties on our inverse dynamics results, we built a skeletal model with accurate segment masses and moments of inertia (see above) and imported it into the MuJoCo (Roboti LLC, Redmond, WA, USA) physics engine to solve for internal joint torques (Todorov et al., 2012) (Fig. S2).

RESULTS

Fifty jumps were recorded from four frogs. Only the trials that met the following criteria were included in analysis: (1) the frog did not turn during the jump and hind leg extension was symmetric; (2) the frog took off fully; and (3) all external markers were visible throughout the jump.

Forces exerted during jumps

Peak total force (single foot force×2) exerted during jumping ranged from 1.7 to 4.9×body weight, with an average of 3×body weight (Table 1, Table S2). Maximum vertical force exceeded (84% of trials) and peaked earlier than (90% of trials) maximum horizontal force (Fig. 2). Across all trials, peak mediolateral forces averaged −0.01 N, an order of magnitude lower than mean peak fore–aft forces. Each frog exerted a ventrally directed force before jumping because of its foot resting on the force plate (averaging 22±6% body weight). Both anteroposterior and dorsoventral forces were negative during the jump. Mediolateral forces exhibited high variability but were generally positive early in the jump, becoming negative prior to take-off (Fig. 2A). Thus, frogs pushed downwards, posteriorly and medially against the substrate early in the jump, then pushed downwards, posteriorly and laterally against the ground late in jumping. ANCOVA testing revealed strong positive correlations (P<1×10^{-15}) between higher-angle jumps and both higher dorsoventral and higher total exerted forces (Table S3). In

Journal of Experimental Biology (2017) 220, 1882-1893 doi:10.1242/jeb.155416

Table 2. Three-dimensional joint and body angles, and angular velocities (separated by jump angle) during jumping in *Kassina maculata*

Subject	Mean ankle range (deg)	Mean max. ankle angle (deg)	Mean knee range (deg)	Mean max. knee angle (deg)	Mean hip range (deg)	Mean max. hip angle (deg)	Mean SI range (deg)	Mean max. SI angle (deg)	Mean body range (deg)	Mean max. body angle (deg)
KM03	95	144	101	129	82	132	22	165	20	35
KM04	102	146	108	146	86	152	16	158	14	31
KM05	101	148	112	143	84	140	21	168	15	31
KM06	104	153	110	142	84	136	18	165	14	31
All trials	101	148	108	140	84	140	19	163	16	32

	Mean peak angular velocity (rad s^{-1})				
Jump angle	Ankle	Knee	Hip	SI	Body
Low	36.09	29.22	23.22	9.39	5.09
Mid	50.05	40.22	27.58	10.41	6.17
High	61.47	46.75	33.47	10.07	7.78
All trials	49.39	39.05	27.98	10.06	6.31

SI, sacroiliac.

contrast, there was no correlation between anteroposterior force and jump angle.

Velocity, acceleration, jump angle and distance, and timings

The highest recorded velocity during jumping in *K. maculata* was 2.02 m s^{-1}, with average peak velocity across all trials of 1.36 m s^{-1} (Table 1, Table S2). Scaled to body length, peak velocity across all trials was 33.1 SVL s^{-1}, with a mean of 22.6 SVL s^{-1}. Maximum acceleration recorded across all jumps was 79.5 m s^{-2} with an average peak of 35.6 m s^{-2}. *Kassina maculata* exhibited wide variation in jump angles, ranging from 0.3 to 69 deg, with a mean jump angle of 34 deg. Jump distance averaged 0.19 m, with a maximum distance of 0.34 m recorded. On average, peak total force and peak acceleration occurred 60 ms before take-off, and peak velocity 10 ms before take-off (Table 1). ANCOVA revealed strong correlations (P<0.001) between higher-angle jumps and both increased velocities (absolute and scaled to SVL) and accelerations (Table S3).

Three-dimensional limb kinematics

In 49 of 50 trials, the hip, knee and ankle joints opened in a proximal to distal sequence – the hip opened first, followed by the knee and, finally, the ankle (Fig. 3). For the sole exception (KM03 HOP 09, a high jump), knee and ankle extension began simultaneously. All three joints experienced similar maximum values of extension during jumping (Table 2, Table S2). The sacroiliac angle increased during jumping (angle change of 6–29 deg, maximum extension of 151–173 deg), while body angle (maximum values ranging between 2 and 60 deg) increased early in jumping and then decreased during take-off (Fig. 3). Peak and final body angle increased with increasing jump angle; additionally, initial body angle (posture) was higher with increasing jump angle (Fig. 3E). Joint angular velocities increased at more distal joints and – for the body, and the hip, knee and ankle joints – angular velocities increased with jump angle (Table 2). In contrast, peak angular velocities at the sacroiliac joint were similar at low, intermediate and high-angle jumps.

ANCOVAs demonstrated very strong positive correlations (P<1×10^{-7}) between increasing jump angle and knee and body angles (both range of movement and maximum extension) (Table S3). Additionally, there were significant positive correlations (P<0.05) between jump angles and both range of movement and maximum extension angles at the ankle, hip and sacroiliac joints.

Inverse dynamics: external moment arms

Maximum 3D moment arms were longest to the hip and shortened at increasingly distal joints (Table 3, Table S2); however, these very long moment arms occurred briefly at take-off (Fig. 4A–D) because of rapidly changing GRF vector orientation at the end of the jump, and are not representative of time-averaged external moment arm lengths.

External moment arm lengths varied during jumping (Fig. 4A–D) because of changing GRF vector orientation and postural changes. As illustrated by stick figure plots (Fig. 4E–J), the GRF vector: (1) is close but typically medial and anterior to the TMT; (2) shifts from being lateral to medial of the ankle and hip joints, resulting in a brief shortening of these moment arms during the jump; and (3) is usually medial and posterior to the knee, but closely approaches the joint during jumping, reducing moment arm length.

ANCOVAs demonstrate that maximum moment arm length to all joints decreased with increasing jump angle (Table 3, Table S3).

Inverse dynamics: joint torques

External torque magnitudes are controlled by GRF magnitude and external moment arm length. External moments were higher at the ankle and hip than at the TMT and knee because of the proximity of the GRF vector to the latter joints when exerted forces were highest (Table 3, Table S2). This proximity also explains variable *XY* and *XZ* torque traces at the TMT and knee (Fig. 5C,E), in which the mean trace is unreflective of most individual jumps, compared with more predictable patterns at the ankle and hip (Fig. 5A,B,D,F–H), in which the mean trace does meaningfully reflect the general pattern. Peak *XY* and *XZ* moments are similar at the TMT, ankle and knee; in contrast, *XY* torques are always higher than *XZ* torques at the hip (Table 3, Fig. 5).

Torque directions are controlled by the orientation of the GRF vector and its position relative to the joint (Fig. 5). The ankle and hip exhibited strong negative *XY* torques and strong positive *XZ* torques; in contrast, the knee exhibited primarily positive *XY* torques and negative *XZ* torques (Table 3, Fig. 5). *XY* torques at the TMT change direction (from positive to negative) during jumping (Fig. 5) because of the changing orientation of the GRF (Fig. 6).

Three-dimensional external torque magnitudes increased during higher-angle jumps owing to higher forces being exerted and despite shorter moment arms (Table 3, Table S3). ANCOVAs revealed significant correlations between increased torques and higher jump angles at all joints; however, more vertical jumps were

Journal of Experimental Biology (2017) 220, 1882-1893 doi:10.1242/jeb.155416

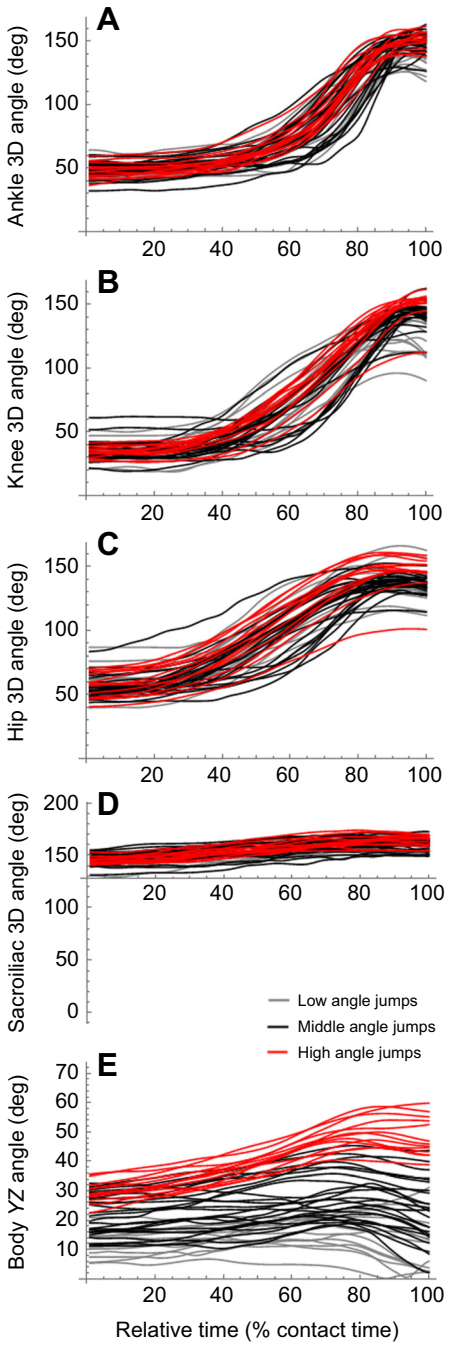

Fig. 3. Joint angles during jumping in *Kassina maculata*. Three-dimensional ankle (A), knee (B), hip (C) and sacroiliac (D) angles and *YZ* body angles (E). Data are normalized and resampled to 100 time points. Trials are separated by jump angle (see Materials and methods): grey traces indicate low-angle jumps; black traces indicate intermediate-angle jumps; red traces indicate high-angle jumps.

strongly correlated (P<0.001) with higher negative (extension) *XY* torques at the ankle and hip, and higher positive (elevation) *XZ* torques at the ankle.

Sensitivity analyses

Joint moments using alternate COP locations are shown in Fig. S1. Patterns resemble those from our original trials, with results converging at take-off owing to the decreasing area of the foot contacting the substrate (i.e. fewer alternate COP locations). For the TMT, ankle and hip joints, torque magnitudes are higher during sensitivity analyses than in original trials because alternate COP locations are always anterior to our estimated COP (the most posterior point of the foot contacting the substrate). As the GRF vector typically passes anterior to these joints, alternate COP locations increase external moment arm lengths and joint torques. Varying COP location does not substantially impact torque patterns or magnitudes at the knee, possibly because the GRF vector passes close to this joint through most of the jump. Discrepancies between original trials and sensitivity analyses increase with higher-angle jumps because of higher forces. In summary, although torque magnitudes early in the jump are affected by alternate COP locations, overall torque patterns are unchanged. Therefore, the sensitivity analysis suggests that errors in the estimated location of the COP do not influence the present findings.

Peak internal torques at the TMT, ankle and knee were an order of magnitude less than external torques during all jumps (Fig. S2). Internal moments at the hip were lower (32–48%) than external moments, but the discrepancy was less than at more distal joints; this is because the bulk of the body mass is being rotated and accelerated at this joint. Average internal moments (throughout the jump) at each joint were an order of magnitude less than average external moments; furthermore, internal moments at the hip, knee and ankle peaked substantially later than external torques. Internal moments at all joints increased during more vertical jump angles.

DISCUSSION

We have presented 3D hind limb kinematics and force data, as well as external moment arms and torques about the hind limb joints, during jumping in *K. maculata* for the first time. We hypothesized that forward thrust for jumps is produced at the hip, knee and ankle whereas elevation is produced at the ankle and knee. Our results generally support our hypothesis; however, we also found that other factors – external moment arm lengths, postural changes in the preparatory phase, faster joint opening and increased joint extension – influenced jump angle as well.

Differential production of thrust and elevation at hind limb joints controls jump angle in *K. maculata*

Our analyses demonstrate that *K. maculata* jumps at angles ranging from nearly horizontal to almost 70 deg. The ability to jump at a range of angles may be important for *K. maculata* when moving through complex, arboreal environments, as demonstrated in tree-dwelling lizards (Toro et al., 2006). How does *K. maculata* modulate jump angle?

Different relative contributions of horizontal and vertical torques at individual hind limb joints partly explain how *K. maculata* achieves a range of jump angles. Three-dimensional torques were highest around the hip and ankle, suggesting muscles acting about these joints are primarily responsible for powering jumps. Negative *XY* torques at the ankle and hip and positive *XY* torques at the knee are consistent with muscles acting to extend these joints in the *XY* plane, generating thrust and pushing the body forward (Fig. 6). Positive *XZ* torques at the ankle and hip and negative *XZ* torques at the knee are consistent with muscles acting to extend these joints in the *XZ* plane, producing elevation and pushing the body upwards (Fig. 6). Our data demonstrate that torques resulting in forward thrust increased substantially at the hip and ankle during steeper jumps, while torques producing elevation increased substantially at the ankle during steeper jumps (Table 3, Table S3). Negative *XY* torques always exceeded positive *XZ* torques at the hip, regardless of jump angle, suggesting most of the work at the hip is forward thrust,

Journal of Experimental Biology (2017) 220, 1882-1893 doi:10.1242/jeb.155416

Table 3. Three-dimensional external moment arms and external torques from inverse dynamics analyses

Subject	Mean max. 3D TMT moment arm (m)	Mean max. 3D ankle moment arm (m)	Mean max. 3D knee moment arm (m)	Mean max. 3D hip moment arm (m)
KM03	0.017±0.005	0.022±0.007	0.032±0.012	0.041±0.019
KM04	0.016±0.005	0.021±0.006	0.031±0.010	0.041±0.018
KM05	0.018±0.004	0.024±0.007	0.028±0.013	0.035±0.018
KM06	0.017±0.004	0.025±0.007	0.039±0.015	0.051±0.020
Low jumps	0.020±0.004	0.027±0.006	0.040±0.009	0.053±0.013
Intermediate jumps	0.017±0.004	0.024±0.007	0.033±0.014	0.043±0.020
High jumps	0.013±0.004	0.018±0.006	0.026±0.012	0.032±0.020
All trials	0.017±0.005	0.023±0.007	0.033±0.013	0.043±0.020
Type	**TMT ext. torque (N.m)**	**Ankle ext. torque (N.m)**	**Knee ext. torque (N.m)**	**Ext. hip torque (N.m)**
Mean max. 3D – all	0.003	0.004	0.003	0.004
Mean max. 3D – low	0.002	0.003	0.003	0.002
Mean max. 3D – intermediate	0.003	0.005	0.003	0.004
Mean max. 3D – high	0.003	0.005	0.004	0.004
Mean max. *XY* – all	0.001	0.001	0.002	0.001
Mean max. *XY* – low	0.001	<0.001	0.002	0.001
Mean max. *XY* – intermediate	0.002	0.001	0.002	0.001
Mean max. *XY* – high	0.002	0.001	0.003	0.001
Mean min. *XY* – all	−0.002	−0.004	−0.001	−0.003
Mean min. *XY* – low	−0.002	−0.003	−0.001	−0.002
Mean min. *XY* – intermediate	−0.002	−0.004	−0.001	−0.003
Mean min. *XY* – high	−0.002	−0.004	−0.001	−0.004
Mean max. *XZ* – all	0.001	0.004	0.001	0.002
Mean max. *XZ* – low	0.001	0.002	<0.001	0.002
Mean max. *XZ* – intermediate	0.001	0.004	0.001	0.003
Mean max. *XZ* – high	0.001	0.004	0.001	0.002
Mean min. *XZ* – all	−0.002	−0.001	−0.002	<−0.001
Mean min. *XZ* – low	−0.001	−0.001	−0.002	−0.001
Mean min. *XZ* – intermediate	−0.002	<−0.001	−0.002	<−0.001
Mean min. *XZ* – high	−0.002	<−0.001	−0.003	<−0.001

as reported by Astley and Roberts (2014) in *Rana*. Our findings also agree with those of Kargo et al. (2002), which suggest horizontal take-off velocity (thrust) is most sensitive to hip extensor torques. In contrast, the ankle contributes equally to thrust and elevation; inverse kinematics (IK) analysis also predicted that ankle extension drives steeper jumps, particularly early in the jump (Richards et al., 2017). Our findings largely support our hypothesis – forward thrust is produced primarily at the hip and ankle whereas elevation is produced primarily at the ankle.

Results for the knee were more complicated: both positive and negative *XY* and *XZ* torques significantly increased with jump angle (Table S3). Again, this in line with IK analysis predicting knee extension is important in increasing take-off angles late in the jump (Richards et al., 2017). Increased torque magnitudes were due to higher forces; variability in torque direction was due to the volatile position of the GRF vector relative to the knee. Kargo et al. (2002) predicted that increased degrees of freedom at the knee joint allows frogs to bring the foot under the body and doubles the ankle extensor torque producing vertical acceleration of the body. Similarly, IK analysis predicted reorientation of the knee rotation axis is crucial to achieving COM elevation (Richards et al., 2017). Thus, fluctuations in torque direction may reflect the subtle and important role of knee positioning in modulating jump angle by permitting high elevation torques to be produced at the ankle. Alternatively (or additionally), close alignment of the GRF vector to the knee joint may increase the effective mechanical advantage of the muscles crossing this joint throughout jumping (see more below).

Lastly, as the frog pushes laterally against the substrate in the final moments before take-off, the GRF vector becomes medially directed, resulting in *XY* and *XZ* torque directions being reversed at the hip and ankle joints during some trials (Figs 5, 6), potentially aiding extension of these joints during take-off.

Moment arms and kinematics influence jump angle in *K. maculata*

Our data show that, in addition to differential joint torques, decreased external moment arm lengths, postural changes, faster joint opening and greater joint extension also play a role in achieving high jump angles. External moment arm length decreased during steeper jumps. Based on lever mechanics:

$$\mathbf{EMA} = \mathbf{r}/\mathbf{R}, \quad (9)$$

in which **EMA** is a muscle's 'effective mechanical advantage', **r** is the muscle moment arm length (presumably unchanged during jumping in frogs; Lieber and Brown, 1992; Kargo and Rome, 2002; Astley and Roberts, 2011), and **R** is the external moment arm (Biewener, 1989). Closer alignment of the limb to the GRF vector during higher-angle jumps in frogs results in a shorter **R** and increases **EMA**, thus helping the frog's muscles to counter the higher GRFs associated with steeper jumps. We also found that ankle moment arm shortens as the joint begins to extend (between time points 70 and 90; Figs 3, 4), leading to increased EMA. This is similar to data presented by Astley and Roberts (2014) from *Rana*, and is crucial to their proposed dynamic catch mechanism, although the decrease in moment arm in *K. maculata* is less pronounced than in *Rana*. Roberts et al. (2011) demonstrated that some frog species are more likely to use power amplification by elastic recoil than others; it is possible that, as a secondary walker, this mechanism is not as important during jumping in *K. maculata* as in *Rana*.

Postural differences also characterized steeper jumps in *K. maculata*. Higher body angles were very strongly correlated

Journal of Experimental Biology (2017) 220, 1882-1893 doi:10.1242/jeb.155416

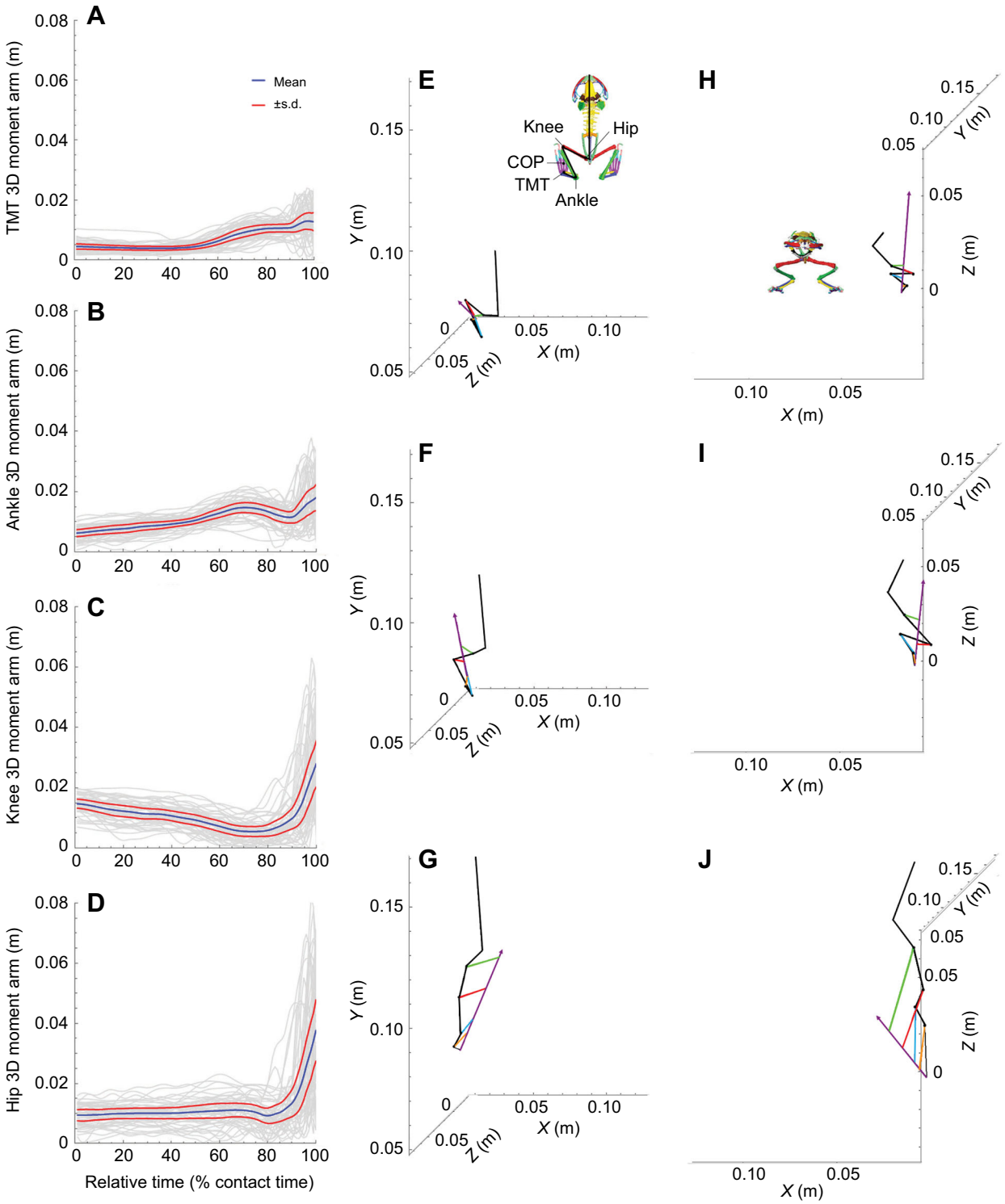

Fig. 4. External moment arms about hind limb joints during jumping in *Kassina maculata*. Three-dimensional external moment arms about the tarsometatarsal (TMT) (A), ankle (B), knee (C) and hip (D) joints; data are normalized and resampled to 100 time points and shown to the same scale. For A–D, blue traces indicate mean moment arm lengths; red traces indicate standard deviations; traces for individual trials are shown in grey. Stick figure plots (E–J) show the frog's body and left hind limb in dorsal (E–G) and anterior (H–J) views as segments, the ground reaction force (GRF) vector (in purple) and external moment arms from the hind limb joints during an exemplar, intermediate-angle jump (KM04 HOP 09) at 44 ms (E,H), 184 ms (F,I) and 240 ms (G,J) into the jump.

with steeper jumps; specifically, higher-angle jumps featured higher-angle starting postures, controlled by the degree of arm extension (Wang et al., 2014). Videos demonstrate that during low-angle jumps, the frog's forearm is nearly parallel to the trackway and the elbow points laterally; in contrast, the forearm is at a steep angle to the trackway and the elbow positioned under the body at the beginning of high-angle jumps. High-speed video and angular velocities (Table 2) demonstrate that, during high-angle jumps, frogs rapidly pitched their bodies backwards prior to limb extension; higher body rotational velocities during steep jumps were also

Journal of Experimental Biology (2017) 220, 1882-1893 doi:10.1242/jeb.155416

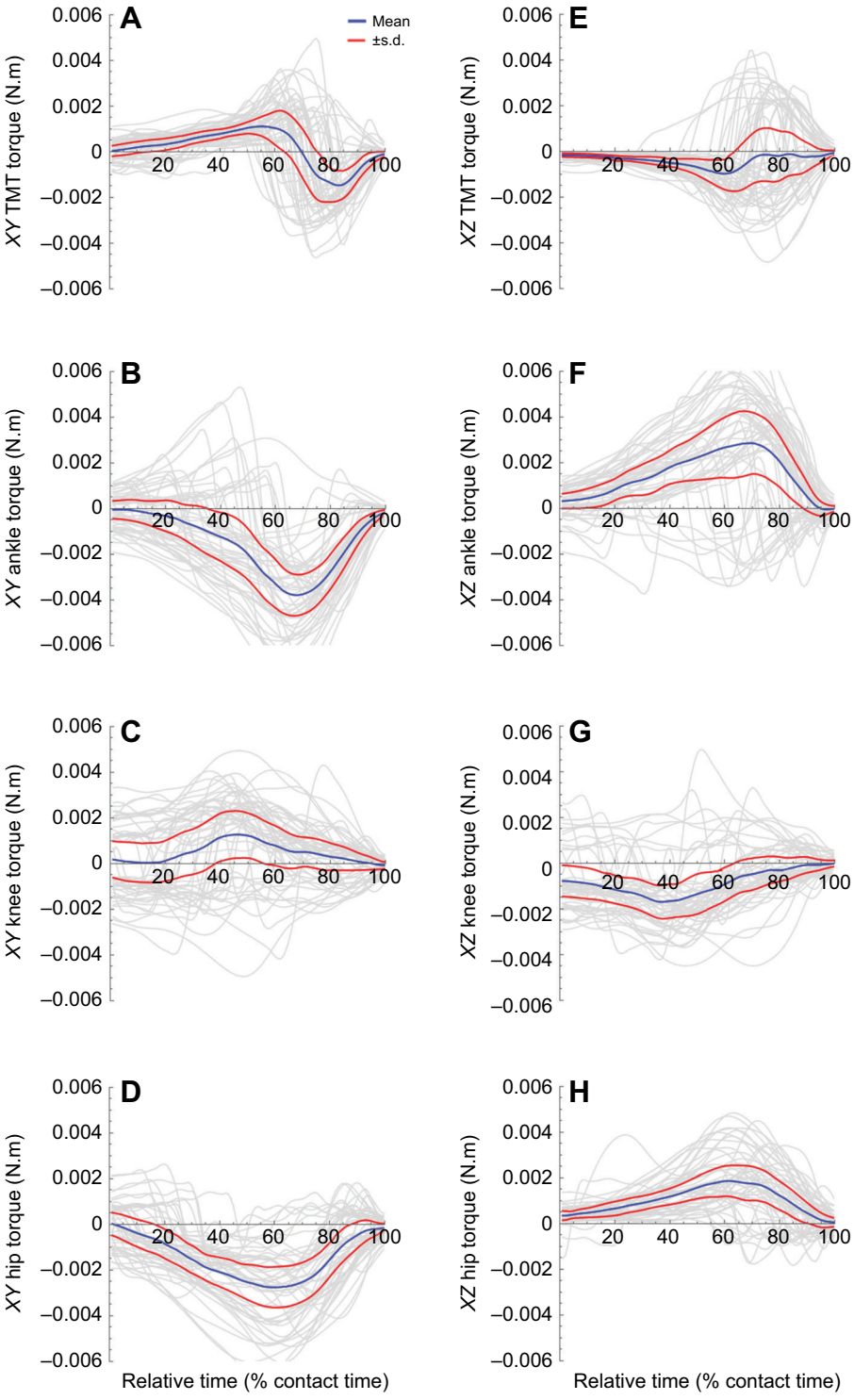

Fig. 5. External torques about the hind limb joints during jumping in *Kassina maculata*. Torques about the tarsometatarsal (TMT) (A,E), ankle (B,F), knee (C,G) and hip (D,H) joints for in the *XY* (horizontal, A–D) and *XZ* planes (transverse vertical, E–H). For *XY* torques, negative values indicate retraction of the segment relative to the body (from the muscle's point of view). For *XZ* torques, positive values indicate adduction of the segment relative to the body. Data are normalized and resampled to 100 time points and are shown to the same scale. Blue traces indicate mean values; red traces indicate standard deviations; traces for individual trials are shown in grey.

observed by Richards et al. (2017). Kargo et al. (2002) demonstrated, using forward dynamic simulations, that take-off angle was most sensitive to long-axis rotation (of the femur) at the hip; although we cannot quantify internal rotation of limb bones using our methods, tilting of the body at the hip joint may play an important role in achieving high-angle jumps in *K. maculata*.

Various force and kinematic parameters were correlated with steeper jumps. Although some low and intermediate angle jumps featured high forces, all high-angle jumps featured increased ventrally directed force. Thus, our findings suggest frogs can choose to exert more force during shallow jumps to increase distance, but they must exert higher forces to jump at steep angles. The ankle, knee and hip joints opened faster during more vertical jumps, and increased jump angle was also correlated with increased range of movement and extension of these joints, particularly the knee (also see Richards et al., 2017). Greater extension of the knee and hip joints during more vertical jumps was also reported by Lutz and Rome (1996a). We also found significant correlation of increased extension of the sacroiliac joint during steeper jumps, supporting hypotheses of sacroiliac function by Emerson and De

Journal of Experimental Biology

Journal of Experimental Biology (2017) 220, 1882-1893 doi:10.1242/jeb.155416

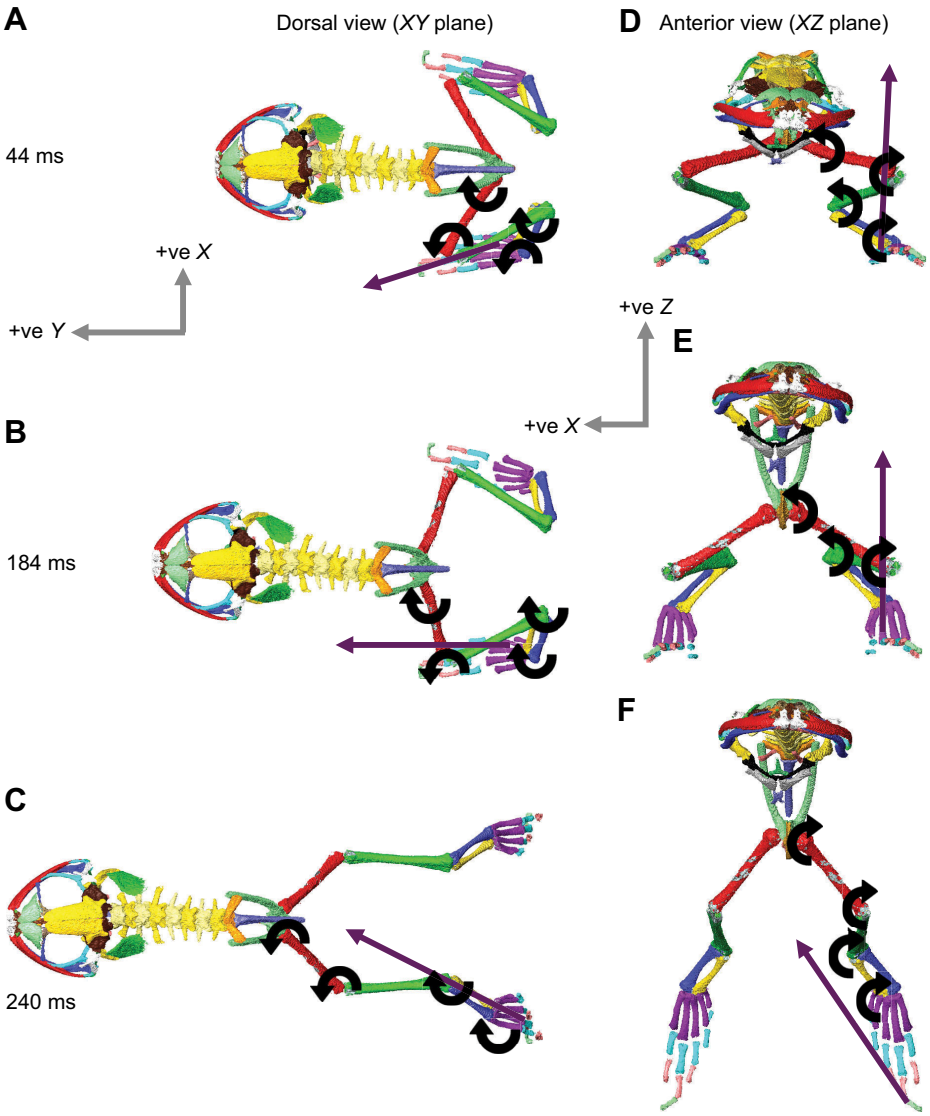

Fig. 6. External torques about the hind limb joints of *Kassina maculata* during jumping. Three-dimensional skeletal models of *K. maculata* in dorsal (A–C) and anterior (D–F) views, with global coordinates shown; forelimbs are not included in the models. Postures are based on external kinematic data from KM04 HOP 09. Models show the frog early in the jump (A,D), in mid-jump (B,E) and just prior to take-off (C,F). Purple arrows shows the direction (but not magnitude) of the ground reaction force (GRF) in the *XY* and *XZ* planes. Curved black arrows show the direction of the external moment produced at the joint by the GRF.

Jongh (1980); but unlike the body and hind limb joints, angular velocity at this joint did not increase with steeper jump angles (see also Richards et al., 2017).

Thus, our data demonstrate that external moment arm lengths, preparatory posture and kinematic differences also help explain how *K. maculata* achieves a wide range of jump angles. Results from IK analysis suggest that dynamic modulation of joint rotation axes during the jump are an additional means by which frogs can control jump angle (Richards et al., 2017).

Kassina maculata jumping performance is similar to that of other frog species

We cannot rigorously test whether morphological or behavioural adaptations for walking in some frogs compromise jumping performance using a single-species test, particularly as there are limited data available for non-walking hyperoliids. Furthermore, previous studies span a restricted range of taxonomic groups and vary in experimental methodology, reported anatomical and performance metrics, animal size, temperature and motivation. Nonetheless, we can compare our jump performance metrics from *K. maculata* with similar data collected from other anurans (Table 4).

The peak resultant exerted force (multiplied by two and scaled to body mass) for *K. maculata* was above the average of the reported range (Table 4). Peak vertical force both exceeded and occurred earlier than peak horizontal force in *K. maculata*, similar to ranids (Calow and Alexander, 1973; Nauwelaerts and Aerts, 2006; Astley and Roberts, 2014; Wang et al., 2014) but unlike hylids (Marsh and John-Alder, 1994). Maximum take-off velocities in *K. maculata* were slightly below average velocity reported in other frogs, whereas jump distance (scaled to SVL) was within the range reported for ranids but substantially lower than distances recorded in hylids (Table 4). The proximal to distal pattern of joint opening observed during jumping in *K. maculata* has been widely reported among frogs (Calow and Alexander, 1973; Peters et al., 1996; Nauwelaerts and Aerts, 2003; Astley and Roberts, 2014; Wang et al., 2014) and is thought to maximize foot-to-ground contact time, prolong acceleration (so that maximum velocity is reached as late as possible) and aid in elastic energy pre-storage (Bobbert and van Ingen Schenau, 1988; van Ingen Schenau, 1989; Wang et al., 2014). Range of movement and maximum values of extension for the ankle, knee, hip and sacroiliac joints in *K. maculata* are similar to those reported in other species (Calow and Alexander, 1973; Lutz and Rome, 1996a; Peters et al., 1996; Nauwelaerts and Aerts, 2003; Astley and Roberts, 2014). Jump angle in *K. maculata* averaged 34 deg, within the range reported in other frogs (Table 4) but lower than the optimal angle of 42 deg thought to maximize jump distance

Journal of Experimental Biology (2017) 220, 1882-1893 doi:10.1242/jeb.155416

Table 4. Jumping performance metrics in *Kassina maculata* compared with other frog taxa for which comparable data are available

Taxa	Peak GRF (single-foot force×2/body mass)	Peak velocity (SVL)	Max. jump distance (SVL)	Mean jump angle (deg)	Jump angle range (deg)
Bombina[1,14]	4.2	31–43	n/a	n/a	n/a
Bufo[2]	n/a	n/a	n/a	31	14–51
Melanophryniscus[14]	2.3	23	n/a	n/a	n/a
Phrynoidis[14]	4.9	26	n/a	n/a	n/a
Anaxyrus[14]	2.6	16	n/a	n/a	n/a
Scaphiopus[14]	3.3	30	n/a	n/a	n/a
Hylids (five species)[3,4,14]	6.5	45–115	13–32	40	n/a
Phyllomedusa[14]	2.4	28	n/a	n/a	n/a
Litoria[14]	5.2	52	n/a	n/a	n/a
Kassina maculata	4.9	33	6	34	0.3–69
Kassina senegalensis[14]	3.8	30	n/a	n/a	n/a
Heterixalus[14]	2.7	37	n/a	n/a	n/a
Phrynomantis[14]	2.2	20	n/a	n/a	n/a
Kaloula[14]	3	20	n/a	n/a	n/a
Rana catesbeiana[3, 5,6]	n/a	15	6	42	~10–60
Rana dybowskii[7]	2	n/a	5	n/a	~35–50
Rana esculenta[8,9]	2.7	n/a	n/a	40	n/a
Rana nigromaculata[1]	n/a	53	n/a	n/a	n/a
Rana pipiens[10–12]	4.8	56	9	26	16–42
Rana temporaria[13]	3.6	n/a	n/a	34	n/a
Rana rugosa[1]	n/a	50	n/a	n/a	n/a
Polypedates[14]	6	46	n/a	n/a	n/a

[1]Choi and Park, 1996; [2]Gillis and Biewener, 2000; [3]Marsh, 1994; [4]Marsh and John-Alder, 1994; [5]Olson and Marsh, 1998; [6]Astley et al., 2013; [7]Wang et al., 2014; [8]Nauwelaerts and Aerts, 2003; [9]Nauwelaerts and Aerts, 2003; [10]Hirano and Rome, 1984; [11]Lutz and Rome, 1996a; [12]Astley and Roberts, 2014; [13]Calow and Alexander, 1973; [14]Astley, 2016.

(Marsh, 1994). *Kassina maculata* are also capable of achieving a relatively wide range of jump angles (nearly 70 deg) compared with those reported in other frogs (Table 4).

In terms of these performance metrics and limited comparative data from other frogs, *K. maculata* appears to be an average jumper. Our results suggest that presumed anatomical/behavioural adaptations for walking in *K. maculata* do not affect jumping performance (but see Astley, 2016), echoing studies that demonstrate limited evidence for a performance trade-off between jumping and swimming (Emerson and De Jongh, 1980; Peters et al., 1996; Nauwelaerts et al., 2007; Herrel et al., 2014; Astley, 2016). It should be noted, however, that *K. maculata* is not morphologically specialized for walking to the degree found in other taxa (some microhylids, brevicepitines or hemisotids); thus, it is unknown how adaptation to walking may affect jumping performance more generally among frogs.

Conclusions

The results presented here document force and joint kinematics during jumping in *K. maculata*, as well as results from inverse dynamics analysis of the hind limb. We show that forward thrust is generated primarily at the hip and ankle, while increased elevation (permitting steeper jumps) is generated primarily at the ankle. Additionally, postural changes – including body angle in the preparatory phase and positioning of the knee – as well as decreased external moment arm length, faster joint opening and increased joint extension allow higher-angle jumps in this taxon. Furthermore, our data suggest jumping performance in *K. maculata* is not compromised by secondary adaptation to walking and running. Finally, we conducted sensitivity analyses that demonstrate: (1) alternate COP locations during take-off result in increased torque magnitudes early in the jump, but do not impact overall patterns of joint torques; and (2) peak internal torques are an order of magnitude lower than external torques at distal hind limb joints, and can be considered negligible. Internal torque magnitudes at the hip are 32–48% of external torque magnitudes.

One limitation of our methods is the inability to visualize movements of internal structures. Previous studies (e.g. Kargo et al., 2002) have suggested the importance of long-axis rotations of hind limb bones during jumping; in contrast, Astley and Roberts (2014) found that such movements were minimal. Investigating such movements and their impact awaits future experiments using X-ray reconstruction of moving morphology (XROMM).

Postural changes (tilting of the body due to extension of the arms that causes rotation of the pelvis relative to the femur, and knee positioning) appear to be a major control on jump angle in *K. maculata*. Many of the major muscles that power jumping originate on the lateral aspect of the ilium and insert at or distal to the knee (Prikyl et al., 2009); thus, variations in starting posture at different jump angles would change the moment arms and, potentially, the action of these muscles. Indeed, Kargo and Rome (2002) demonstrated that frog hind limb muscles have different functions depending on task and limb configuration. Future XROMM experiments and musculoskeletal modelling will allow us to explore internal rotations of the limb segments during jumping and permit detailed models of muscle function in jumping frogs, including how morphological changes during the evolution of frogs may have impacted locomotor evolution. Ultimately, work from both living and fossil anurans can be used to understand the origin of frog musculoskeletal anatomy and locomotor behaviour, and whether frog limbs were indeed built for jumping, walking or multi-functionality, with the ability to adapt to varying movements and terrains.

Acknowledgements

Alastair Wallis (RVC) cared for research animals. Steve Amos, Emily Sparkes and Timothy West (RVC) assisted with obtaining software and equipment, and the experimental setup. Special thanks to Vivian Allen (RVC) for his help in determining segment moment of inertia. Robert Asher, Matthew Mason and Colin Shaw (University of Cambridge) provided CT-scanning time. Technical support for Avizo was provided by Alejandra Sánchez-Eróstegui and Jean Luc-Garnier (FEI Visualization Sciences Group).

Competing interests
The authors declare no competing or financial interests.

Author contributions
L.B.P., A.J.C. and C.T.R. designed the research. E.A.E. and L.B.P. constructed the experimental setup. K.P.C. built the original force plate. C.T.R. and L.B.P. wrote the LabVIEW script to collect force data. All authors collected *in vivo* experimental data. L.B.P. carried out CT-scanning and processed CT data. L.B.P. and C.T.R. wrote Mathematica scripts for data processing. L.B.P. carried out inverse dynamics analyses. C.T.R. developed code to calculate internal torques. L.B.P. drafted the manuscript. All authors read and commented on the manuscript.

Funding
Funding was provided by an European Research Council Starting Grant to C.T.R. (PIPA 338271, Paleo-robotics and the innovations of propulsion in amphibians). Funding for K.P.C was provided by the Leverhulme Trust.

Supplementary information
Supplementary information available online at
http://jeb.biologists.org/lookup/doi/10.1242/jeb.155416.supplemental

References
Ahn, A. N., Furrow, E. and Biewener, A. A. (2004). Walking and running in the red-legged running frog, *Kassina maculata*. *J. Exp. Biol.* **207**, 399-410.
Alexander, R. McN. (1995). Leg design and jumping technique for humans, other vertebrates and insects. *Phil. Trans. R. Soc. Lond. B.* **347**, 235-248.
Allen, V., Bates, K. T., Li, Z. and Hutchinson, J. R. (2013). Linking the evolution of body shape and locomotor biomechanics in bird-line archosaurs. *Nature* **497**, 104-107.
Astley, H. C. (2016). The diversity and evolution of locomotor muscle properties in anurans. *J. Exp. Biol.* **219**, 3163-3173.
Astley, H. C. and Roberts, T. J. (2011). Evidence for a vertebrate catapult: elastic energy storage in the plantaris tendon during frog jumping. *Biol. Lett.* **8**, 386-389.
Astley, H. C. and Roberts, T. J. (2014). The mechanics of elastic loading and recoil in anuran jumping. *J. Exp. Biol.* **217**, 4372-4378.
Astley, H. C., Abbott, E. M., Azizi, E., Marsh, R. L. and Roberts, T. J. (2013). Chasing maximal performance: a cautionary tale from the celebrated jumping frogs of Calaveras County. *J. Exp. Biol.* **216**, 3847-3953.
Azizi, E. and Roberts, T. J. (2010). Muscle performance during frog jumping: influence of elasticity on muscle operating lengths. *Proc. Biol. Soc.* **277**, 1523-1530.
Biewener, A. A. (1989). Scaling body support in mammals: limb posture and muscle mechanics. *Science* **245**, 45-48.
Biewener, A. (2003). *Animal Locomotion.* Oxford: Oxford University Press.
Biltz, R. M. and Pellegrino, E. D. (1969). The chemical anatomy of bone. I. A comparative study of bone composition in sixteen vertebrates. *J. Bone Joint Surg. Am.* **51**, 456-466.
Bobbert, M. F. and van Ingen Schenau, G. J. (1988). Coordination in vertical jumping. *J. Biomech.* **21**, 249-262.
Calow, L. and Alexander, R. McN. (1973). A mechanical analysis of a hind limb of a frog. *J. Zool. Lond.* **171**, 292-321.
Choi, I.-H. and Park, K. (1996). Variation in take-off velocity of anuran amphibians: relation to morphology, muscle contractile function and enzyme activity. *Comp. Biochem. Physiol.* **4**, 393-400.
Danos, N. and Azizi, E. (2015). Passive stiffness of hindlimb muscles in anurans with distinct locomotor specializations. *Zoology* **118**, 239-247.
Emerson, S. B. (1978). Allometry and jumping in frogs: helping the twain to meet. *Evolution* **32**, 551-564.
Emerson, S. (1979). The ilio-sacral articulation in frogs: form and function. *Biol. J. Linn. Soc.* **11**, 153-168.
Emerson, S. B. (1982). Frog postcranial morphology: identification of a functional complex. *Copeia* **3**, 603-613.
Emerson, S. B. and De Jongh, H. J. (1980). Muscle activity at the ilio-sacral articulation of frogs. *J. Morph.* **166**, 129-144.
Gillis, G. B. and Biewener, A. A. (2000). Hindlimb extensor muscle function during jumping and swimming in the toad (*Bufo marinus*). *J. Exp. Biol.* **203**, 3547-3563.
Hedrick, T. L. (2008). Software techniques for two- and three-dimensional kinematic measurements of biological and biomimetic systems. *Bioinspir. Biomim.* **3**, 034001.
Herrel, A., Vasilopoulou-Kampitsi, M. and Bonneaud, C. (2014). Jumping performance in the highly aquatic frog, *Xenopus tropicalis*: sex-specific relationships between morphology and performance. *PeerJ* **2**, e661.
Hirano, M. and Rome, L. (1984). Jumping performance of frogs (*Rana pipiens*) as a function of muscle temperature. *J. Exp. Biol.* **108**, 429-439.
Jenkins, F. A. and Shubin, N. H. (1998). *Prosalirus bitis* and the anuran caudopelvic mechanism. *J. Vert. Paleontol.* **18**, 495-510.
Kamel, L. T., Peters, S. E. and Bashor, D. P. (1996). Hopping and swimming in the leopard frog, *Rana pipiens:* II. A comparison of muscle activities. *J. Morph.* **230**, 17-31.
Kargo, W. J. and Rome, L. C. (2002). Functional morphology of proximal lindlimb muscles in the frog *Rana pipiens*. *J. Exp. Biol.* **205**, 1987-2004.
Kargo, W. J., Nelson, F. and Rome, L. C. (2002). Jumping frogs: assessing the design of the skeletal system by anatomically realistic modelling and forward dynamics simulation. *J. Exp. Biol.* **205**, 1683-1702.
Lieber, R. L. and Brown, C. G. (1992). Sarcomere length-joint angle relationships of seven frog hindlimb muscles. *Aca Anat.* **145**, 289-295.
Loveridge, J. P. (1976). Strategies of water conservation in southern African frogs. *Zool. Africana.* **11**, 319-333.
Lutz, G. J. and Rome, L. C. (1996a). Muscle function during jumping frogs. I. Sarcomere length change, EMG pattern, and jumping performance. *Am. J. Physiol.* **271**, C563-C570.
Lutz, G. J. and Rome, L. C. (1996b). Muscle function during jumping frogs. II. Mechanical properties of muscle: implications for system design. *Am. J. Physiol.* **271**, C571-C578.
Marsh, R. (1994). Jumping ability of anuram amphibians. In *Advances in Veterinary Science and Comparative Medicine: Comparative Vertebrate Exercise Physiology*, Vol. 38 (ed. J. H. Jones), pp. 51-111. New York: Academic Press.
Marsh, R. and John-Alder, H. (1994). Jumping performance of hylid frogs measured with high-speed cine film. *J. Exp. Biol.* **188**, 131-141.
McAllister, W. and Channing, A. (1983). Comparison of toe pads of some southern African climbing frogs. *S. African J. Zool.* **18**, 110-114.
Nauwelaerts, S. and Aerts, P. (2003). Propulsive impulse as a covarying performance measure in the comparison of the kinematics of swimming and jumping in frogs. *J. Exp. Biol.* **2-6**, 4341-4351.
Nauwelaerts, S. and Aerts, P. (2006). Take-off and landing forces in jumping frogs. *J. Exp. Biol.* **209**, 66-77.
Nauwelaerts, S., Ramsay, J. and Aerts, P. (2007). Morphological correlates of aquatic and terrestrial locomotion in a semi-aquatic frog, *Rana esculenta:* no evidence for a design conflict. *J. Anat.* **210**, 304-317.
Olson, J. and Marsh, R. (1998). Activation patterns and length changes in hindlimb muscles of the bullfrog *Rana catesbeiana* during jumping. *J. Exp. Biol.* **201**, 2763-2777.
Peplowski, M. M. and Marsh, R. L. (1997). Work and power output in the hindlimb muscles of Cuban tree frogs *Osteopilus septentrionalis* during jumping. *J. Exp. Biol.* **200**, 2861-2870.
Peters, S., Kamel, L. and Pashor, D. (1996). Hopping and swimming in the leopard frog, *Rana pipiens:* I. Step cycles and kinematics. *J. Morph.* **230**, 1-16.
Prikyl, T., Aerts, P., Havelová, P., Herrel, A. and Rocek, Z. (2009). Pelvic and thigh musculature on frogs (Anura) and origin of anuram jumping locomotion. *J. Anat.* **214**, 100-139.
Reilly, S. and Jorgensen, M. (2011). The evolution of jumping in frogs: morphological evidence for the basal anuran locomotor condition and the radiation of locomotor systems in crown group anurans. *J. Morph.* **272**, 149-168.
Richards, C. T., Porro, L. B. and Collings, A. J. (2017). Kinematic control of extreme jump angles in the red-legged running frog, *Kassina maculata*. *J. Exp. Biol.* **220**, 1894-1904.
Roberts, T. J. and Marsh, R. L. (2003). Probing the limits to muscle-powered accelerations: lessons from jumping bullfrogs. *J. Exp. Biol.* **206**, 2567-2580.
Roberts, T. J., Abbott, E. M. and Azizi, E. (2011). The weak link: do muscle properties determine locomotor performance in frogs? *Phil. Trans. R. Soc. B.* **366**, 1488-1495.
Todorov, E., Erez, T. and Tassa, Y. (2012). MuJoCo: A physics engine for model-based control. In *Proceedings of the 2012 IEEE/RSJ International Conference on Intelligent Robots and Systems*. IEEE.
Toro, E., Herrel, A. and Irschick, D. J. (2006). Movement control strategies during jumping in a lizard (*Anolis valencienni*). *J. Biomech.* **39**, 2014-2016.
van Ingen Schenau, G. (1989). From rotation to translation: constraints on multi-joint movements and the unique action of bi-articular muscles. *Hum. Mov. Sci.* **8**, 301-337.
Wang, Z., Ji, A., Endlein, T., Samuel, D., Yao, N., Wang, Z. and Dai, Z. (2014). The role of fore- and hindlimbs during jumping in the Dybowski's frog (*Rana dybowskii*). *J. Exp. Zool.* **321A**, 324-333.
Weisstein, E. (2009). Point-Line Distance–3-Dimensional. *From MathWorld–A Wolfram Web Resource*. http://mathworld.wolfram.com/Point-LineDistance3-Dimensional.html.
Wilson, R. S., Franklin, C. E. and James, R. S. (2000). Allometric scaling relationships pf jumping performance in the striped marsh frog *Limnodynastes peronii*. *J. Exp. Biol.* **203**, 1937-1946.
Zug, G. (1972). Anuran locomotion: structure and function, I. Preliminary observations on the relation between jumping and osteometrics of appendicular and postaxial skeleton. *Copeia.* **4**, 613-624.